NANO · MICRO small
www.small-journal.com

Uncovering the Mechanism Behind the Improved Stability of 2D Organic–Inorganic Hybrid Perovskites

Zhiming Shi, Zhen Cao, Xiaojuan Sun, Yuping Jia, Dabing Li, Luigi Cavallo, and Udo Schwingenschlögl**

2D organic–inorganic hybrid perovskites (OIHPs) may resolve the stability problem of bulk OIHPs. First-principles calculations are employed to investigate the mechanism behind their favorable material properties. Two processes are identified to play a critical role: First, the 2D structure supports additional distortions that enhance the intrinsic structural stability. Second, the surface terminations of 2D OIHPs suppress degradation effects due to humidity. Having uncovered the stabilization mechanism, 2D OIHPs are designed with optimal stability and favorable electronic properties.

Organic–inorganic hybrid perovskites (OIHPs) have outstanding potential in light harvesting devices.[1–8] Important properties include the direct bandgap, low carrier effective mass, defect tolerance, high charge mobility, long lifetime, and low-cost fabrication.[3–6] The power conversion efficiency of solar cells based on OIHPs has improved from 3.8% in 2009,[9] in several steps,[10–19] to 23.2% in 2018.[20] In spite of this quick progress, there remain two great challenges that hinder large-scale commercial applications. The first problem is the toxicity of Pb, which calls for strategies to develop Pb-free OIHPs.[21–26] The second problem is the poor long-term stability of the materials, which has both intrinsic thermodynamic[27,28] and environment-induced[12,29–31] origins. In this context, it has been demonstrated that the introduction of Cs cations[32,33] and the replacement of methylammonium (MA^+) with formamidinium (FA^+) cations[33–35] in I-based OIHPs are promising approaches to improve the stability.

Recently, Ruddlesden–Popper 2D OIHPs attract interest due to an enhanced resistance against humidity combined with power conversion efficiencies comparable to bulk OIHPs. For example, $PEA_2MA_2Pb_3I_{10}$ (PEA = $C_6H_5(CH_2)_2NH_3^+$) can resist 52% relative humidity more than twice as long as $MAPbI_3$.[29] While the power conversion efficiency of $MAPbI_3$ is found to decrease to 40% after 24 h and then slowly to less than 10% after 2250 h, $BA_2MA_3Pb_4I_{13}$ (BA = $CH_3(CH_2)_3NH_2^+$) retains 80% after 200 h and 70% after 2050 h.[36] The general structure of 2D $S_2A_{n-1}M_nX_{3n+1}$ OIHPs (S: spacer ammonium cation, A: bulk cation, M: metal, and X: halogen) is illustrated in **Figure 1**. Synthesis of high-quality samples with n = 1, 2, 3, 4, and 5 and the dependence of their electronic properties on the thickness n have been reported in Refs. [37–39]. Excellent performance in solar cells has been demonstrated in Refs. [40–42] and other applications have been discussed in Refs. [43–45].

However, basic understanding of the mechanisms behind the enhanced stability is strongly limited. In general, the stability of a material is determined by 1) its intrinsic structure[46,47] and 2) potential reactions with the environment.[48,49] We use in the present work first-principles calculations to study the roles of the different structural components for the stability of 2D OIHPs and for their electronic properties. The migration process of H_2O from the surface into the bulk is explored in detail, employing the migration barrier as index to evaluate the material stability. We develop insights into the factors determining the stability of 2D OIHPs, which will allow us to identify materials (with comparable or even improved electronic properties) that are significantly more stable than $BA_2MA_{n-1}Pb_nI_{3n+1}$ and $PEA_2MA_{n-1}Pb_nI_{3n+1}$.

First-principles calculations are performed employing the generalized gradient approximation (Perdew–Burke–Ernzerhof parametrization, PBE) and projector-augmented wave method.[50] An onsite interaction is considered for the Pb 6s orbital to overcome the self-interaction error, using the experimental bandgap of Ref. [51] as indicator to determine the value of the onsite parameter. It turns out that an onsite parameter of 7.5 eV results in excellent agreement, with theoretical (experimental) bandgaps of 2.50 eV (2.44 eV) for BA_2PbI_4, 2.34 eV (2.16 eV) for $BA_2MAPb_2I_7$, 2.16 eV (2.05 eV) for $BA_2MA_2Pb_3I_{10}$, 1.93 eV (1.92 eV) for $BA_2MA_3Pb_4I_{13}$, and 2.50 eV (2.44 eV) for $BA_2MA_4Pb_5I_{16}$. The van der Waals interaction[52,53] is also included in the calculations in agreement with previous work.[54] The simulation cells for the 2D OIHPs are built with vacuum slabs thicker than 15 Å to avoid artificial interaction of periodic images. We employ 5 × 5 × 1 and 15 × 15 × 1 Monkhorst–Pack k-grids in the structural

Dr. Z. M. Shi, Prof. X. J. Sun, Dr. Y. P. Jia, Prof. D. B. Li
State Key Laboratory of Luminescence and Applications
Changchun Institute of Optics
Fine Mechanics and Physics
Chinese Academy of Sciences
3888 Dongnanhu Road, Changchun 130033, P. R. China
E-mail: lidb@ciomp.ac.cn
Dr. Z. M. Shi, Dr. Z. Cao, Prof. L. Cavallo, Prof. U. Schwingenschlögl
King Abdullah University of Science and Technology (KAUST)
KAUST Solar Center (KSC)
Thuwal 23955-6900, Kingdom of Saudi Arabia
E-mail: udo.schwingenschlogl@kaust.edu.sa
The ORCID identification number(s) for the author(s) of this article can be found under https://doi.org/10.1002/smll.201900462.

DOI: 10.1002/smll.201900462

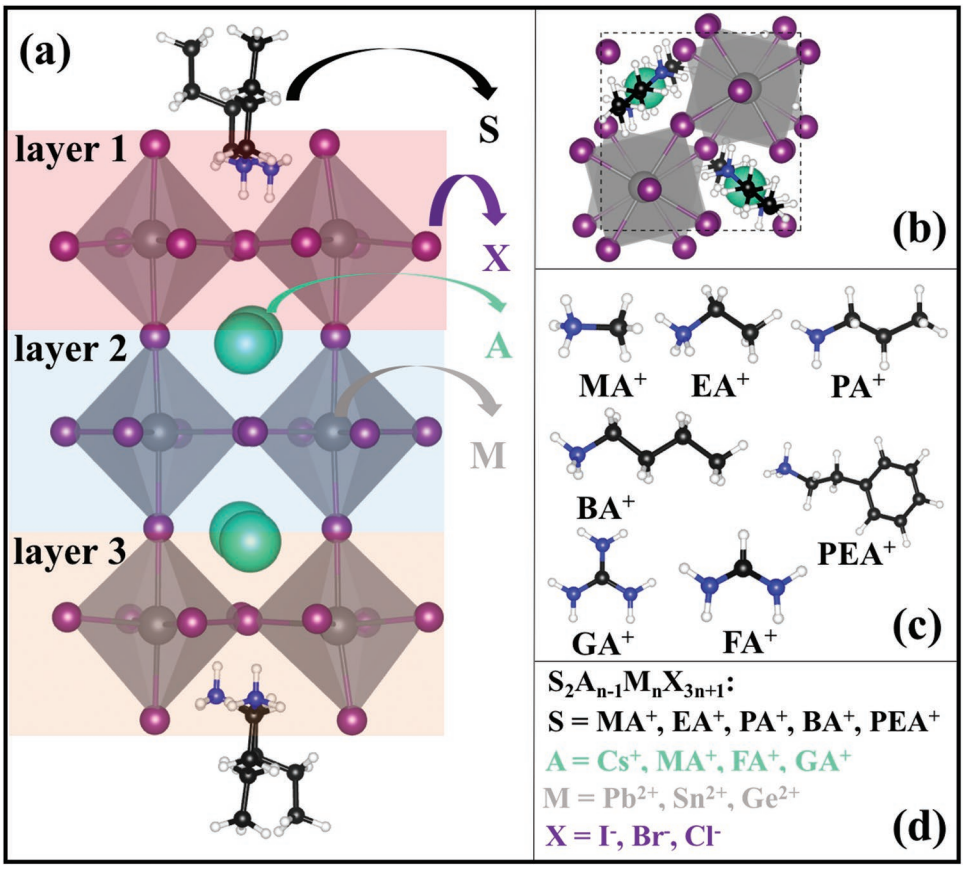

Figure 1. a) Side and b) top views of the $S_2A_2M_3X_{10}$ structure, showing in-plane distortions of the M-centered octahedra. Layers 1 and 3 form the surface. c) Structures of the amine molecules. d) Possible compositions.

relaxations and self-consistent calculations, respectively, and 51 k-points between high symmetry points of the Brillouin zone in the band structure calculations. In addition, the force and total energy convergence thresholds are set to 0.01 eV Å^{-1} and 10^{-6} eV, respectively. H_2O migration barriers are obtained by means of the climbing image nudged elastic band method,[55,56] using 12 images to connect the initial and final configurations (force convergence 0.05 eV Å^{-1}). Finally, 2 × 2 supercells are used for ab-initio molecular dynamics simulations at 300 K (NVT ensemble, Nosé–Hoover thermostat, total simulation time 10 ps, time step of 1 fs).

Bulk $MAPbI_3$ exists in tetragonal and orthorhombic phases, the former being energetically favorable at room temperature.[57] Our calculations confirm this order for BA_2PbI_4, with an energy difference of 0.31 eV per formula unit. For this reason, we will consider the tetragonal phase in the following. As previous work indicates that $n = 3$ is sufficient to model the (001) surface, we will investigate the structural and electronic properties of $S_2A_2M_3X_{10}$ slab configurations,[58] as shown in Figure 1, considering at the S and A sites methylammonium (MA^+), ethylammonium (EA^+), propylammonium (PA^+), butylammonium (BA^+), phenylethylammonium (PEA^+), guanidinium (GA^+), and formamidinium (FA^+), at the M site Pb^{2+}, Sn^{2+}, and Ge^{2+}, and at the X site Cl-, Br^-, and I^-. In each case, the material stability will be compared with that of $BA_2MA_2Pb_3I_{10}$ and $PEA_2MA_2Pb_3I_{10}$, for which we obtain lattice constants of a = 8.76 Å and b = 8.68 Å, i.e., about 2% smaller than the experimental values[39] due to the finite temperature in the experiment. **Table 1** lists the obtained lattice constants for all the considered structures, showing that the S, A, and M sites have only little effects in contrast to the X site (lattice constants decrease from I^- to Br^- by 0.42 Å and from Br^- to Cl^- by 0.63 Å).

For A = MA, M = Pb, and X = I, 2D OIHPs decompose into the monoiodides of the spacer ammonium cations (SI) and methylammonium iodide (MAI) as well as PbI_2. The formation energy

$$E_f = \frac{E - 2E_{\mathrm{SI}} - (n-1)E_{\mathrm{MAI}} - nE_{PbI_2}}{n} \tag{1}$$

associated with this process is used to evaluate the intrinsic structural stability (negative values indicate stable structures). While E is the total energy of the 2D OIHP, E_{SI}, E_{MAI}, and E_{PbI2} are the total energies per formula unit of molecular SI, molecular MAI, and bulk PbI_2, respectively. All these energy values are obtained after structural relaxation, employing the same computational setup. In **Figure 2**a, we present results for E_f of $MA_2MA_{n-1}Pb_nI_{3n+1}$ in comparison to the calculated values for experimentally realized $BA_2MA_{n-1}Pb_nI_{3n+1}$ and $PEA_2MA_{n-1}Pb_nI_{3n+1}$ for thicknesses of $n = 1$, 2, 3, 4, and 5 layers. In each case, the values are less negative for $MA_2MA_{n-1}Pb_nI_{3n+1}$, implying lower intrinsic stability. According to Equation (1),

Table 1. Lattice constants, bandgap, and effective mass of $S_2A_2M_3X_{10}$.

	Lattice constants [Å]		Bandgap [eV]		Effective mass [m_e]	
	a	*B*	PBE	PBE + SOC + U	hole	electron
$MA_2MA_2Pb_3I_{10}$	8.74	8.72	2.00	2.12	0.28	0.28
$EA_2MA_2Pb_3I_{10}$	8.75	8.73	2.00	2.11	0.27	0.25
$PA_2MA_2Pb_3I_{10}$	8.78	8.73	2.00	2.11	0.28	0.29
$BA_2MA_2Pb_3I_{10}$	8.76	8.68	1.99	2.16	0.28	0.31
$PEA_2MA_2Pb_3I_{10}$	8.73	8.67	2.00	2.13	0.28	0.30
$BA_2Cs_2Pb_3I_{10}$	8.77	8.67	1.93	2.10	0.23	0.23
$BA_2FA_2Pb_3I_{10}$	8.99	8.76	1.93	2.01	0.25	0.27
$BA_2GA_2Pb_3I_{10}$	8.98	8.97	1.88	1.98	0.24	0.25
$BA_2MA_2Ge_3I_{10}$	8.69	8.56	1.37	–	0.29	0.26
$BA_2MA_2Sn_3I_{10}$	8.74	8.67	1.03	–	0.14	0.29
$BA_2MA_2Pb_3Cl_{10}$	8.13	8.02	2.80	3.21	0.36	0.47
$BA_2MA_2Pb_3Br_{10}$	8.34	8.22	2.36	2.67	0.32	0.43

this difference must be due to the term $E - 2E_{SI}$, i.e., related to the spacer ammonium cations. The exothermic energies from BA to BAI and PEA to PEAI are larger than that from MA to MAI, demonstrating that the spacer ammonium cations affect the stability of the material. The fact that the curves in Figure 2a increase with the thickness *n* (to the corresponding bulk values) indicates that reduction of the dimension enhances the intrinsic stability of the materials. This effect can be attributed to additional structural distortions in thinner slabs, similar to the finding that the tetragonal phase of $BA_2Pb_1I_4$ is energetically favorable over the orthorhombic phase due in-plane and out-of-plane octahedral distortions, see Figure 2b,c. Suppression of the out-of-plane distortions in 2D OIHPs with increasing thickness *n* results in internal stress and thus in reduced stability.

While it is known that bulk OIHPs are sensitive to humidity, the exact effect of H_2O on the stability of 2D OIHPs is not clear. Understanding the atomic mechanism how H_2O molecules interact with 2D OIHPs, however, is critical for developing strategies of materials design. It has been demonstrated experimentally that $MAPbI_3$ films decompose in the presence of H_2O in a three-step process, specifically 1) formation of $MAPbI_3 \cdot H_2O$, 2) partial degradation into $MA_4PbI_6 \cdot 2H_2O$, and 3) complete degradation into MAI and PbI_2 with release of H_2O molecules[59]

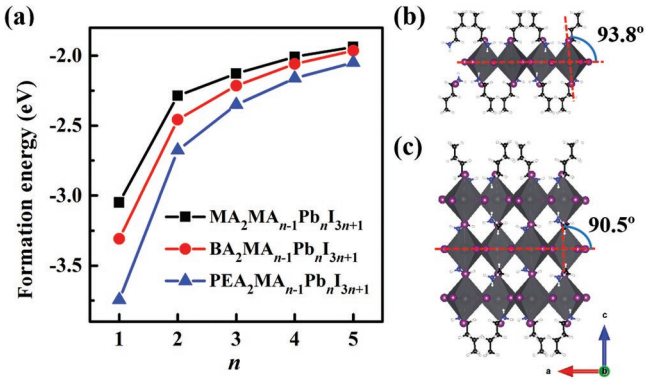

Figure 2. a) Formation energy as function of the thickness *n*. Top and side views of b) orthorhombic and c) tetragonal $BA_2Pb_1I_4$. The tilting angles are marked.

$$MAPbI_3 + H_2O \rightarrow MAPbI_3 \cdot H_2O \tag{2}$$

$$MAPbI_3 \cdot H_2O \rightarrow \frac{1}{4}MA_4PbI_6 \cdot 2H_2O + \frac{1}{2}H_2O + \frac{3}{4}PbI_2 \tag{3}$$

$$\frac{1}{4}MA_4PbI_6 \cdot 2H_2O \rightarrow MAI + \frac{1}{2}H_2O + \frac{1}{4}PbI_2 \tag{4}$$

As 2D OIHPs are characterized by their hydrophobic spacer ammonium cations, we now investigate the migration process of H_2O molecules from the surface into the bulk by the climbing image nudged elastic band method and by ab-initio molecular dynamics simulations. The same computational methodology has been applied to the bulk materials in Ref. [58]. According to the data given in **Figure 3**a, we obtain in the case of $BA_2MA_2Pb_3I_{10}$ a migration barrier of 0.72 eV, much higher than that of $MA_2MA_2Pb_3I_{10}$ (0.13 eV).[58] Initially, the H atoms of the H_2O molecule prefer pointing to the surface I atoms because of Coulombic interaction. During infiltration this interaction weakens and H bonds are formed to the spacer ammonium cations. The energy cost to break the H bonds determines the migration barrier together with the serious structural distortions of the octahedral framework that develop when the H_2O molecule moves. Turning to Figure 3b, the case of $PEA_2MA_2Pb_3I_{10}$ is more complicated due the benzene ring of PEA^+. Crossing of the H_2O molecule through the benzene ring requires to overcome a barrier of 0.16 eV and yields a total energy gain of 0.02 eV by the formation of H bonds to the NH_2^+ group. The structural distortions of the octahedral framework then lead to a migration barrier of 0.64 eV. Bond lengths and angles in the initial, transition, and final structures of the climbing image nudged elastic band calculations are summarized in Figure S1 and Table S1 in the Supporting Information. We note that the effects of H_2O infiltration on

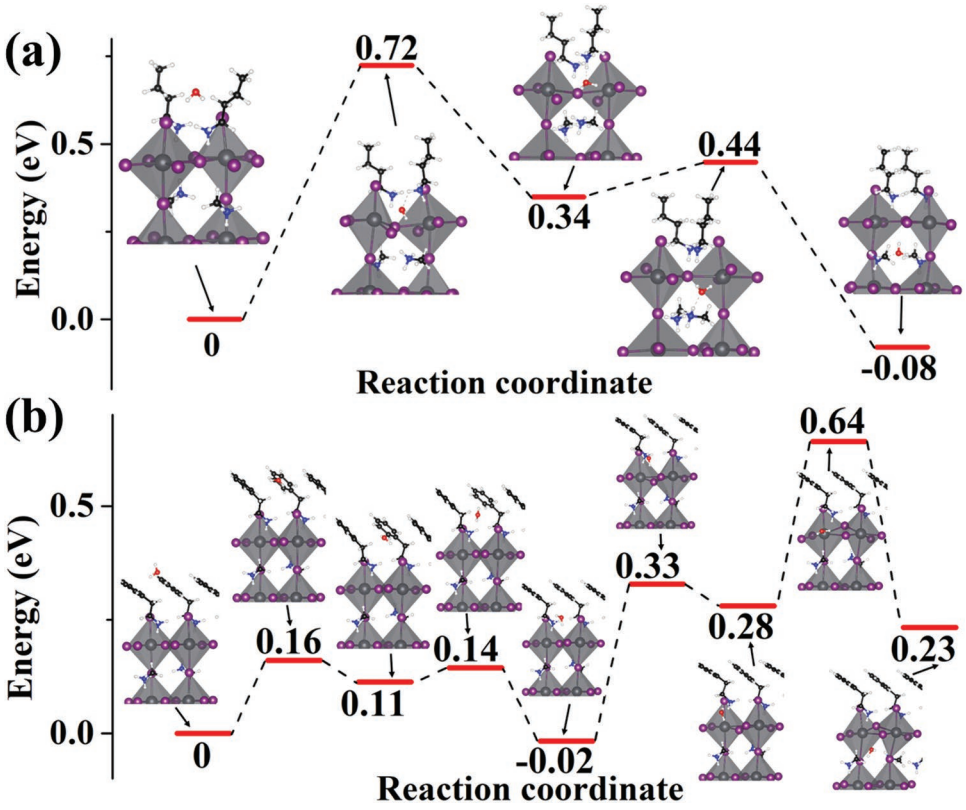

Figure 3. Migration of H_2O from the surface into the bulk of a) $BA_2MA_2Pb_3I_{10}$ and b) $PEA_2MA_2Pb_3I_{10}$.

the electronic properties are comparable to those reported for $MA_2MA_2Pb_3I_{10}$.[51]

Resistance against humidity is also seen in ab-initio molecular dynamics simulations in that we cover the materials with liquid water. **Figure 4**a–c gives snapshots of the structures in the end of our simulations for $MA_2MA_2Pb_3I_{10}$, $BA_2MA_2Pb_3I_{10}$, and $PEA_2MA_2Pb_3I_{10}$. For $MA_2MA_2Pb_3I_{10}$ the MA molecules on the surface tend to diffuse into the water and the outmost octahedra show serious distortions, see the green-dashed circles in Figure 4a. On the other hand, no such distortions are observed for $BA_2MA_2Pb_3I_{10}$ and $PEA_2MA_2Pb_3I_{10}$, reflecting excellent structural stability. We find that the H_2O molecules hardly cross

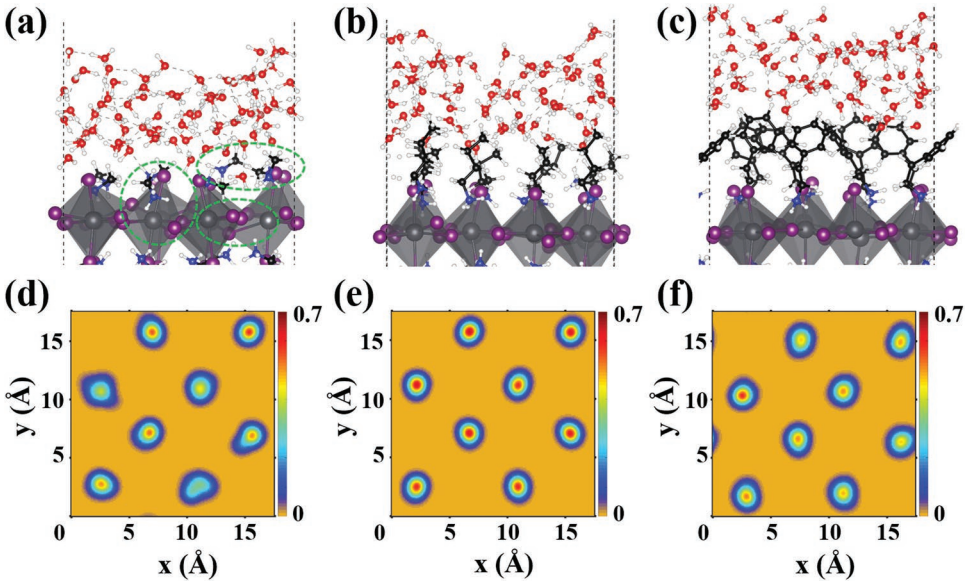

Figure 4. Snapshots in the end of ab-initio molecular dynamics simulations for a) $MA_2MA_2Pb_3I_{10}$, b) $BA_2MA_2Pb_3I_{10}$, and c) $PEA_2MA_2Pb_3I_{10}$ covered with H_2O molecules. Probability maps of the horizontal positions of the outmost I atoms are given in panels (d–f), respectively.

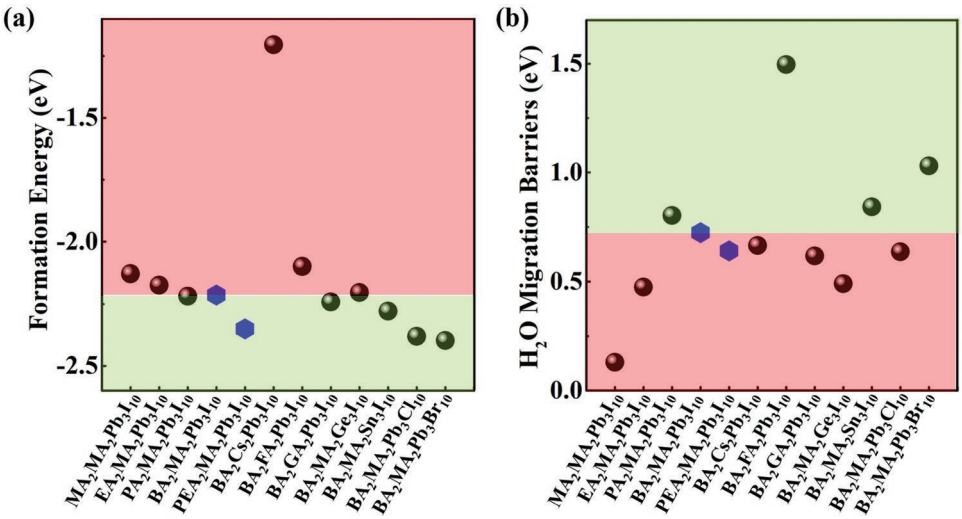

Figure 5. a) Formation energy and b) H_2O migration barrier. Experimentally realized materials are given as blue hexagons for reference. Green/red background color distinguishes regions in which the formation energy or H_2O migration barrier is favorable/unfavorable as compared to the best experimental material.

the spacer ammonium cations and therefore do not affect the octahedral framework. Probability maps of the horizontal positions of the outmost I atoms in Figure 4d–f show large displacements for $MA_2MA_2Pb_3I_{10}$, while for $BA_2MA_2Pb_3I_{10}$ and $PEA_2MA_2Pb_3I_{10}$ the I atoms remain close to their equilibrium positions.

MA^+, EA^+, and PA^+ spacer ammonium cations lead to migration barriers of 0.13 eV for $MA_2MA_2Pb_3I_{10}$, 0.48 eV for $EA_2MA_2Pb_3I_{10}$, and 0.80 eV for $PA_2MA_2Pb_3I_{10}$, see **Figure 5**b, showing that the migration barrier increases with growing length of the hydrocarbon chain up to three C atoms. Short hydrocarbon chains, on the other hand, allow the H_2O molecules to approach the octahedral framework easily and the fact that such spacer ammonium cations may move and/or rotate helps to release energy from structural distortions. While longer hydrocarbon chains can stabilize 2D OIHPs, shorter chains and more conductive ligands aid optoelectronic applications. The intrinsic structural stability can be evaluated in terms of the formation energy. $PA_2MA_2Pb_3I_{10}$, $BA_2GA_2Pb_3I_{10}$, $BA_2MA_2Sn_3I_{10}$, $BA_2MA_2Pb_3Cl_{10}$, and $BA_2MA_2Pb_3Br_{10}$ show lower values, see the green region in Figure 5a, than $BA_2MA_2Pb_3I_{10}$. On the other hand, the H_2O migration barriers of $PA_2MA_2Pb_3I_{10}$, $BA_2FA_2Pb_3I_{10}$, $BA_2MA_2Sn_3I_{10}$, and $BA_2MA_2Pb_3Br_{10}$ are higher than that of $BA_2MA_2Pb_3I_{10}$, see the green region in Figure 5b, reflecting more resistance against humidity. Both improved intrinsic structural stability and resistance against humidity are found for $PA_2MA_2Pb_3I_{10}$, $BA_2MA_2Sn_3I_{10}$, and $BA_2MA_2Pb_3Br_{10}$. The second of these materials does not contain Pb and, notably, has been realized experimentally in Ref. [60]. We obtain for the Sn^{4+} decomposition pathway of $BA_2MA_2Sn_3I_{10}$

$$BA_2MA_2Sn_3I_{10} + \frac{3}{2}O_2 \rightarrow 2BAI + 2MAI + \frac{3}{2}SnI_4 + \frac{3}{2}SnO_2 \quad (5)$$

much higher E_f than for the Sn^{2+} decomposition pathway (–0.09 eV as compared to –2.28 eV), indicating that Sn^{4+} decomposition dominates. The negative value point to potential of experimental realization.

The bandgaps, effective masses, and adsorption coefficients of the different 2D OIHPs are compared in **Figure 6**, see also Table 1. In Figure 6a we give bandgaps obtained on the PBE level, considering spin–orbital coupling (PBE + SOC) and additionally an onsite interaction for the Pb 6s orbital (PBE + SOC + U). It turns out that SOC effects (reduction of the size of the bandgap) are much smaller for $BA_2MA_2Ge_3I_{10}$ and $BA_2MA_2Sn_3I_{10}$ than for the Pb-based materials. On the PBE + SOC + U level the bandgap of 2.16 eV for $BA_2MA_2Pb_3I_{10}$ decreases to 1.37 eV for $BA_2MA_2Ge_3I_{10}$ and 1.03 eV for $BA_2MA_2Sn_3I_{10}$ but increases to 3.21 eV for $BA_2MA_2Pb_3Cl_{10}$ and 2.67 eV for $BA_2MA_2Pb_3Br_{10}$. On the other hand, the size of the bandgap is little affected by the S and A sites, as they hardly contribute to the states at the band edges. For the same reason, the effective mass varies only between 0.23 and 0.30 m_e, see Figure 6b. $BA_2MA_2Sn_3I_{10}$ shows the smallest hole effective mass of 0.14 m_e. For $BA_2MA_2Pb_3Cl_{10}$ and $BA_2MA_2Pb_3Br_{10}$ the carrier effective masses are found to be larger than for $BA_2MA_2Pb_3I_{10}$. Figure 6c gives adsorption coefficients calculated on the PBE + SOC + U level, the results being consistent with the above trends of the bandgaps. Focusing on the three identified materials with improved stability, $PA_2MA_2Pb_3I_{10}$ resembles the features of $BA_2MA_2Pb_3I_{10}$, while the bandgap is reduced for $BA_2MA_2Sn_3I_{10}$ and enhanced for $BA_2MA_2Pb_3Br_{10}$.

We have studied the mechanisms leading to improved stability of 2D OIHPs as compared to bulk OIHPs by calculating formation energies and H_2O migration barriers. We have demonstrated that reduction of the dimension enhances the intrinsic stability due to introduction of additional structural degrees of freedom. On the other hand, the spacer ammonium cations, in particular those with long hydrophobic hydrocarbon chains, stabilize 2D OIHPs by separating H_2O from the octahedral framework. We also have succeeded to identify three candidate materials, $PA_2MA_2Pb_3I_{10}$, $BA_2MA_2Sn_3I_{10}$, and $BA_2MA_2Pb_3Br_{10}$, that exhibit both better intrinsic structural

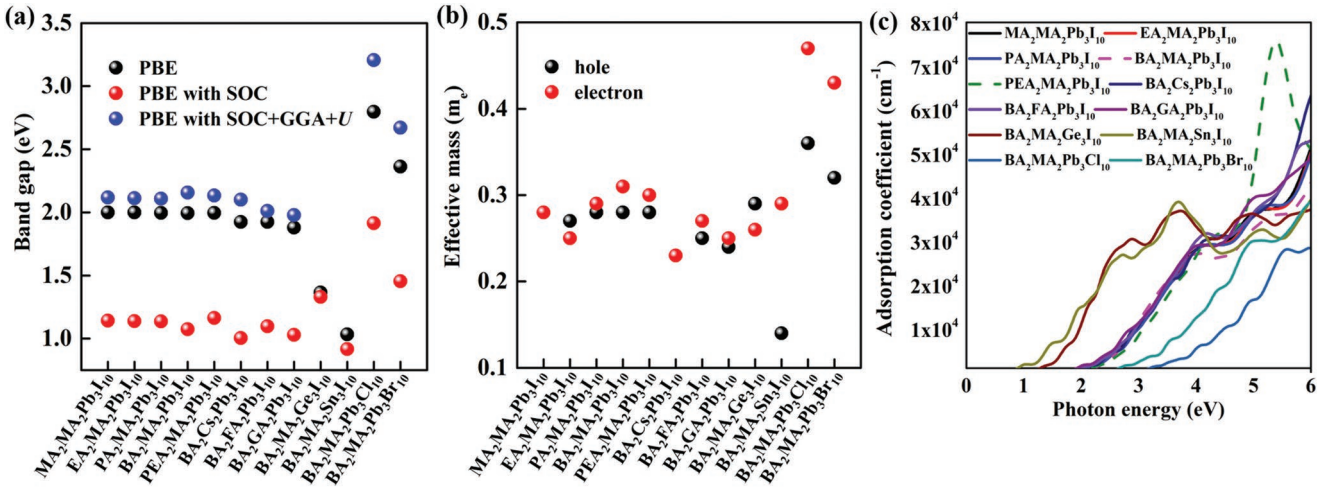

Figure 6. a) Bandgap, b) effective mass, and c) adsorption coefficient. The dashed lines represent the experimentally realized structures.

stability and resistance against humidity as compared to experimentally studied $BA_2MA_2Pb_3I_{10}$. $BA_2MA_2Sn_3I_{10}$ is of special interest, as it does not contain toxic Pb.

Supporting Information

Supporting Information is available from the Wiley Online Library or from the author.

Acknowledgements

The research reported in this publication was supported by funding from National Science Fund for Distinguished Young Scholars (61725403), King Abdullah University of Science and Technology (KAUST), Special Fund for Research on National Major Research Instruments (61827813), National Natural Science Foundation of China (61874118, 61574142, 61834008, and 61804152), Key Program of the International Partnership Program of CAS (181722KYSB20160015), Special Project for Inter-Government Collaboration of the State Key Research and Development Program (2016YFE0118400), Jilin Provincial Science & Technology Department (20180201026GX), CAS Interdisciplinary Innovation Team, Youth Innovation Promotion Association of CAS, CAS Research Instruments Development project, and CAS Pioneer Hundred Talents Program. For computer time, this research used the resources of the Supercomputing Laboratory at KAUST and National Supercomputing Center in Wuxi.

Conflict of Interest

The authors declare no conflict of interest.

Keywords

2D hybrid perovskite, first-principles calculation, solar cell, stability

Received: January 26, 2019
Revised: February 23, 2019
Published online:

[1] L. Etgar, P. Gao, Z. Xue, Q. Peng, A. K. Chandiran, B. Liu, M. K. Nazeeruddin, M. Grätzel, *J. Am. Chem. Soc.* **2012**, *134*, 17396.
[2] M. M. Lee, J. Teuscher, T. Miyasaka, T. N. Murakami, H. J. Snaith, *Science* **2012**, *338*, 643.
[3] G. Xing, N. Mathews, S. Sun, S. S. Lim, Y. M. Lam, M. Grätzel, S. Mhaisalkar, T. C. Sum, *Science* **2013**, *342*, 344.
[4] C. C. Stoumpos, C. D. Malliakas, M. G. Kanatzidis, *Inorg. Chem.* **2013**, *52*, 9019.
[5] C. Wehrenfennig, G. E. Eperon, M. B. Johnston, H. J. Snaith, L. M. Herz, *Adv. Mater.* **2014**, *26*, 1584.
[6] C. S. Ponseca Jr., T. J. Savenije, M. Abdellah, K. Zheng, A. Yartsev, T. Pascher, T. Harlang, P. Chabera, T. Pullerits, A. Stepanov, J. Wolf, V. Sundström, *J. Am. Chem. Soc.* **2014**, *136*, 5189.
[7] C. Xie, P. You, Z. Liu, L. Li, F. Yan, *Light: Sci. Appl.* **2017**, *6*, e17023.
[8] L. Gu, Z. Fan, *Light: Sci. Appl.* **2017**, *6*, e17090.
[9] A. Kojima, K. Teshima, Y. Shirai, T. Miyasaka, *J. Am. Chem. Soc.* **2009**, *131*, 6050.
[10] H.-S. Kim, C.-R. Lee, J.-H. Im, K.-B. Lee, T. Moehl, A. Marchioro, S.-J. Moon, R. Humphry-Baker, J.-H. Yum, J. E. Moser, M. Grätzel, N. Park, *Sci. Rep.* **2012**, *2*, 591.
[11] J. Burschka, N. Pellet, S.-J. Moon, R. Humphry-Baker, P. Gao, M. K. Nazeeruddin, M. Grätzel, *Nature* **2013**, *499*, 316.
[12] J. H. Noh, S. H. Im, J. H. Heo, T. N. Mandal, S. I. Seok, *Nano Lett.* **2013**, *13*, 1764.
[13] N. J. Jeon, J. H. Noh, Y. C. Kim, W. S. Yang, S. Ryu, S. I. Seok, *Nat. Mater.* **2014**, *13*, 897.
[14] J.-H. Im, I.-H. Jang, N. Pellet, M. Grätzel, N.-G. Park, *Nat. Nanotechnol.* **2014**, *9*, 927.
[15] W. S. Yang, J. H. Noh, N. J. Jeon, Y. C. Kim; S. Ryu, J. Seo, S. I. Seok, *Science* **2015**, *348*, 1234.
[16] W. Chen, Y. Wu, Y. Yue, J. Liu, W. Zhang, X. Yang, H. Chen, E. Bi, I. Ashraful, M. Grätzel, L. Han, *Science* **2015**, *350*, 944.
[17] M. Saliba, T. Matsui, K. Domanski, J.-Y. Seo, A. Ummadisingu, S. M. Zakeeruddin, J.-P. Correa-Baena, W. R. Tress, A. Abate, A. Hagfeldt, M. Grätzel, *Science* **2016**, *354*, 206.
[18] H. Tan, A. Jain, O. Voznyy, X. Lan, F. P. G. De Arquer, J. Z. Fan, R. Quintero-Bermudez, M. Yuan, B. Zhang, Y. Zhao, F. Fan, P. Li, L. N. Quan, Y. Zhao, Z. -H. Lu, Z. Yang, S. Hoogland, E. H. Sargent, *Science* **2017**, *355*, 722.
[19] Y. Zheng, J. Kong, D. Huang, W. Shi, L. McMillon-Brown, H. E. Katz, J. Yu, A. D. Taylor, *Nanoscale* **2018**, *10*, 11342.
[20] N. J. Jeon, H. Na, E. H. Jung, T.-Y. Yang, Y. G. Lee, G. Kim, H.-W. Shin, S. I. Seok, J. Lee, J. Seo, *Nat. Energy* **2018**, *3*, 682.

[21] D. B. Mitzi, C. Feild, W. Harrison, A. Guloy, *Nature* **1994**, *369*, 467.
[22] F. Hao, C. C. Stoumpos, D. H. Cao, R. P. Chang, M. G. Kanatzidis, *Nat. Photonics* **2014**, *8*, 489.
[23] N. K. Noel, S. D. Stranks, A. Abate, C. Wehrenfennig, S. Guarnera, A.-A. Haghighirad, A. Sadhanala, G. E. Eperon, S. K. Pathak, M. B. Johnston, A. Petrozza, L. M. Herza, H. J. Snaith, *Energy Environ. Sci.* **2014**, *7*, 3061.
[24] P. P. Boix, S. Agarwala, T. M. Koh, N. Mathews, S. G. Mhaisalkar, *J. Phys. Chem. Lett.* **2015**, *6*, 898.
[25] X.-G. Zhao, J.-H. Yang, Y. Fu, D. Yang, Q. Xu, L. Yu, S.-H. Wei, L. Zhang, *J. Am. Chem. Soc.* **2017**, *139*, 2630.
[26] X.-G. Zhao, D. Yang, Y. Sun, T. Li, L. Zhang, L. Yu, A. Zunger, *J. Am. Chem. Soc.* **2017**, *139*, 6718.
[27] B. Conings, J. Drijkoningen, N. Gauquelin, A. Babayigit, J. D'Haen, L. D'Olieslaeger, A. Ethirajan, J. Verbeeck, J. Manca, E. Mosconi, F. D. Angelis, H. Boyen, *Adv. Energy Mater.* **2015**, *5*, 1500477.
[28] J.-H. Yang, W.-J. Yin, J.-S. Park, S.-H. Wei, *J. Mater. Chem. A* **2016**, *4*, 13105.
[29] I. C. Smith, E. T. Hoke, D. Solis-Ibarra, M. D. McGehee, H. I. Karunadasa, *Angew. Chem.* **2014**, *126*, 11414.
[30] G. Niu, W. Li, F. Meng, L. Wang, H. Dong, Y. Qiu, *J. Mater. Chem. A* **2014**, *2*, 705.
[31] J. A. Christians, P. A. Miranda Herrera, P. V. Kamat, *J. Am. Chem. Soc.* **2015**, *137*, 1530.
[32] H. Choi, J. Jeong, H.-B. Kim, S. Kim, B. Walker, G.-H. Kim, J. Y. Kim, *Nano Energy* **2014**, *7*, 80.
[33] J. W. Lee, D. H. Kim, H. S. Kim, S. W. Seo, S. M. Cho, N. G. Park, *Adv. Energy Mater.* **2015**, *5*, 1501310.
[34] G. E. Eperon, S. D. Stranks, C. Menelaou, M. B. Johnston, L. M. Herz, H. J. Snaith, *Energy Environ. Sci.* **2014**, *7*, 982.
[35] D. P. McMeekin, G. Sadoughi, W. Rehman, G. E. Eperon, M. Saliba, M. T. Hörantner, A. Haghighirad, N. Sakai, L. Korte, B. Rech, M. B. Johnston, L. M. Herz, H. J. Snaith, *Science* **2016**, *351*, 151.
[36] H. Tsai, W. Nie, J.-C. Blancon, C. C. Stoumpos, R. Asadpour, B. Harutyunyan, A. J. Neukirch, R. Verduzco, J. J. Crochet, S. Tretiak, L. Pedesseau, J. Even, M. A. Alam, G. Gupta, J. Lou, P. J. Ajayan, M. J. Bedzyk, M. G. Kanatzidis, A. D. Mohite, *Nature* **2016**, *536*, 312.
[37] L. Dou, A. B. Wong, Y. Yu, M. Lai, N. Kornienko, S. W. Eaton, A. Fu, C. G. Bischak, J. Ma, T. Ding, N. S. Ginsberg, L.-W. Wang, A. P. Alivisatos, P. Yang, *Science* **2015**, *349*, 1518.
[38] D. H. Cao, C. C. Stoumpos, O. K. Farha, J. T. Hupp, M. G. Kanatzidis, *J. Am. Chem. Soc.* **2015**, *137*, 7843.
[39] C. C. Stoumpos, D. H. Cao, D. J. Clark, J. Young, J. M. Rondinelli, J. I. Jang, J. T. Hupp, M. G. Kanatzidis, *Chem. Mater.* **2016**, *28*, 2852.
[40] X. Zhang, X. Ren, B. Liu, R. Munir, X. Zhu, D. Yang, J. Li, Y. Liu, D.-M. Smilgies, R. Li, Z. Yang, T. Niu, X. Wang, A. Amassian, K. Zhao, S. Liu, *Energy Environ. Sci.* **2017**, *10*, 2095.
[41] T. Zhang, M. I. Dar, G. Li, F. Xu, N. Guo, M. Grätzel, Y. Zhao, *Sci. Adv.* **2017**, *3*, e1700841.
[42] B. E. Cohen, M. Wierzbowska, L. Etgar, *Adv. Funct. Mater.* **2017**, *27*, 1604733.
[43] G. Xing, N. Mathews, S. S. Lim, N. Yantara, X. Liu, D. Sabba, M. Grätzel, S. Mhaisalkar, T. C. Sum, *Nat. Mater.* **2014**, *13*, 476.
[44] R. Li, C. Yi, R. Ge, W. Zou, L. Cheng, N. Wang, J. Wang, W. Huang, *Appl. Phys. Lett.* **2016**, *109*, 151101.
[45] Z. Yang, O. Voznyy, G. Walters, J. Z. Fan, M. Liu, S. Kinge, S. Hoogland, E. H. Sargent, *ACS Photonics* **2017**, *4*, 830.
[46] J. Haruyama, K. Sodeyama, L. Han, Y. Tateyama, *Acc. Chem. Res.* **2016**, *49*, 554.
[47] J. Carrillo, A. Guerrero, S. Rahimnejad, O. Almora, I. Zarazua, E. Mas-Marza, J. Bisquert, G. Garcia-Belmonte, *Adv. Energy Mater.* **2016**, *6*, 1502246.
[48] B. Hailegnaw, S. Kirmayer, E. Edri, G. Hodes, D. Cahen, *J. Phys. Chem. Lett.* **2015**, *6*, 1543.
[49] G. Niu, X. Guo, L. Wang, *J. Mater. Chem. A* **2015**, *3*, 8970.
[50] G. Kresse, D. Joubert, *Phys. Rev. B* **1999**, *59*, 1758.
[51] J.-C. Blancon, H. Tsai, W. Nie, C. C. Stoumpos, L. Pedesseau, C. Katan, M. Kepenekian, C. M. M. Soe, K. Appavoo, M. Y. Sfeir, S. Tretiak, P. M. Ajayan, M. G. Kanatzidis, J. Even, J. J. Crochet, A. D. Mohite, *Science* **2017**, *355*, 1288.
[52] S. Grimme, *J. Comput. Chem.* **2006**, *27*, 1787.
[53] V. Barone, M. Casarin, D. Forrer, M. Pavone, M. Sambi, A. Vittadini, *J. Comput. Chem.* **2009**, *30*, 934.
[54] A. M. Ganose, C. N. Savory, D. O. Scanlon, *J. Phys. Chem. Lett.* **2015**, *6*, 4594.
[55] D. Sheppard, R. Terrell, G. Henkelman, *J. Chem. Phys.* **2008**, *128*, 134106.
[56] D. Sheppard, P. Xiao, W. Chemelewski, D. D. Johnson, G. Henkelman, *J. Chem. Phys.* **2012**, *136*, 074103.
[57] Y. Kawamura, H. Mashiyama, K. Hasebe, *J. Phys. Soc. Jpn.* **2002**, *71*, 1694.
[58] C.-J. Tong, W. Geng, Z.-K. Tang, C.-Y. Yam, X.-L. Fan, J. Liu, W.-M. Lau, L.-M. Liu, *J. Phys. Chem. Lett.* **2015**, *6*, 3289.
[59] A. I. M. Leguy, Y. Hu, M. Campoy-Quiles, M. I. Alonso, O. J. Weber, P. Azarhoosh, M. Van Schilfgaarde, M. T. Weller, T. Bein, J. Nelson, P. Docampo, P. R. F. Barnes, *Chem. Mater.* **2015**, *27*, 3397.
[60] D. H. Cao, C. C. Stoumpos, T. Yokoyama, J. L. Logsdon, T.-B. Song, O. K. Farha, M. R. Wasielewski, J. T. Hupp, M. G. Kanatzidis, *ACS Energy Lett.* **2017**, *2*, 982.